Article

South Pacific Oscillation contributes to multi-year ENSOs

Check for updates

Xumin Li[1,2,3], Jin-Yi Yu[1] ✉, Ruiqiang Ding[2] ✉, Xiaofeng Xu[3,4], Kai Ji[2] & Tao Wen[2]

Multi-year El Niño-Southern Oscillation (ENSO) events, where the warming (El Niño) or cooling (La Niña) extends beyond a single year, have become increasingly prominent in recent decades. Using observations and climate model simulations, we show that the South Pacific Oscillation (SPO) plays a crucial, previously unrecognized role in determining whether ENSO evolves into a multi-year event. Specifically, when an El Niño (La Niña) triggers a positive (negative) SPO in the extratropical Southern Hemisphere during its decaying phase, the SPO feedbacks onto the tropical Pacific through the wind-evaporation-sea surface temperature mechanism, helping sustain ENSO into a multi-year event. This SPO–ENSO interaction is absent in single-year ENSO events. Furthermore, whether ENSO can trigger the SPO depends systematically on the central SST anomaly location for El Niños and the anomaly intensity for La Niñas, with interference from atmospheric internal variability. These findings highlight the importance of including off-equatorial processes from the Southern Hemisphere in studies of ENSO complexity dynamics.

Recent decades have seen an increasing frequency of multi-year (MY) El Niño-Southern Oscillation (ENSO) events[1–3], where consecutive ENSO events of the same phase persist beyond a single year. Notable cases include the 2018-19-20 El Niño, in which two El Niño events occurred in succession[4], followed by a triple-dip La Niña spanning from 2020 to 2023[5–7]. This prolonged persistence of ENSO in one phase challenges conventional ENSO theories, which primarily describe its oscillatory nature—where El Niño and La Niña events typically alternate, each lasting about a year—resulting in single-year (SY) ENSO events[8,9]. Those traditional ENSO theories, such as the delayed[10,11] and recharge oscillator theories[12,13], explain the alternation between El Niño and La Niña through negative feedback mechanisms in tropical Pacific ocean-atmosphere interactions, particularly the buildup and discharge of equatorial ocean heat content (OHC).

Efforts have been made to refine the traditional ENSO dynamic framework[10–13] to account for the formation of MY ENSO events, by explaining how ENSO duration can be prolonged. For example, DiNezio and Deser[14] demonstrated that incorporating nonlinear dynamics into delayed oscillators can extend ENSO duration beyond a single year. An and Kim[15], along with Im et al.[16], further emphasized the role of nonlinear ocean wave responses to wind in sustaining ENSO events. Iwakiri and Watanabe[17] tuned the recharge oscillation framework with an observed weak recharge efficiency parameter, enabling the dynamic framework to reproduce the occurrence of MY ENSO. Using recharge ENSO dynamics, Wu et al.[18–20]

linked MY La Niña to the substantial OHC discharge caused by a preceding strong El Niño, which often prevents full recharge within a single cycle, leading to a second La Niña. Their work also discovered El Niño onset time related to its duration, with El Niño events that develop early tend to terminate quickly after the mature phase due to the early reflection of delayed negative oceanic feedback.

Efforts have also been made to explore atmosphere-ocean processes in the extratropical Pacific, particularly the North Pacific Meridional Mode (NPMM)[21], as a mechanism for MY ENSO formation[9,22–36]. The role of NPMM in ENSO dynamics was initially highlighted to explain the formation of Central Pacific (CP) ENSO[27,28] whose sea surface temperature anomalies (SSTAs) center more around the International Dateline and influenced more by the variation of northeast trade winds originated from the northern subtropical Pacific but less by the variation of equatorial thermocline variations due to its relatively deeper mean thermocline depth[29]. The NPMM was further suggested to also play a role in the formation of MY ENSO[24]. Specifically, Yu and Fang[24] proposed that El Niño (La Niña) events in the tropical central Pacific can trigger the positive (negative) phase of the NPMM during their decay phase. The SSTAs associated with this NPMM phase can then spread into the tropical central Pacific in the following seasons via the wind-evaporation-SST (WES) feedback mechanism[30], potentially triggering another El Niño (La Niña) and resulting in MY ENSO events. Several additional studies have further

[1]Department of Earth System Science, University of California, Irvine, CA, USA. [2]Key Laboratory of Environmental Change and Natural Disasters of Chinese Ministry of Education, Beijing Normal University, Beijing, China. [3]Key Laboratory of Meteorological Disaster of Ministry of Education (KLME), Nanjing University of Information Science and Technology, Nanjing, China. [4]China Meteorological Administration Training Center, Beijing, China. ✉e-mail: jyyu@uci.edu; drq@bnu.edu.cn

substantiated the contribution of extratropical North Pacific processes to the development of MY ENSO events[23,31,32].

An increasing number of studies have revealed that atmosphere-ocean processes originating from the extratropical South Pacific can also significantly impact ENSO dynamics[33–39]. The South Pacific Meridional Mode (SPMM)[39], the Southern Hemisphere counterpart of the NPMM, was initially identified as a factor influencing the development of Eastern Pacific (EP) ENSO. Li et al.[35] further discovered that ENSO can influence South Pacific sea level pressure (SLP) variability modes, leading to the development of the South Pacific Oscillation (SPO)[38,40], which is a key driver of the SPMM. The SPO, a basin-scale climate mode over the South Pacific, can influence ENSO not only through the SPMM in the southeast Pacific but also via atmosphere-ocean coupling processes in the western Pacific[34,37,41]. These mutual interactions suggest that climate variability in the South Pacific may be initiated by an ENSO event and subsequently feedback to influence its further evolution. As a result, off-equatorial processes from the South Pacific may play a significant role in shaping the formation of MY ENSO events. This possibility has been tentatively examined in several recent case studies, with research showing that the 2020–2023 triple-dip La Niña was largely influenced by South Pacific SST and wind anomalies[5–7,42,43].

Motivated by the proposed relay role of the South Pacific climate modes between ENSO events, this study investigates specifically the potential differentiating impacts of the SPO on the evolution of MY and SY ENSO events. Our research encompasses observational data from 1950 to 2023, Coupled Model Intercomparison Project Phase 6 (CMIP6) historical outputs, and forced atmospheric general circulation model (AGCM) experiments. Our findings reveal that the SPO significantly differentiates between MY and SY ENSO events, both El Niño and La Niña. These results underscore the crucial role of South Pacific climate variability in shaping ENSO evolution patterns.

Results

Significant SPO differences between MY and SY ENSOs

The SPO is characterized by a north-south dipole structure in the South Pacific SLP field, with its positive phase featuring an anomalous low-pressure center over the subtropics and a high-pressure center at higher latitudes (Supplementary Fig. 1)[35,38,40]. We first compared the SPO index (SPOI; see definition in Methods) between MY and SY ENSO events during the second-year boreal spring (February–April, FMA[1]) season (Fig. 1a, b) to examine whether contrasting SPO conditions exist between these two duration groups of ENSO events. In this study, we define Year 0 as the year when the first ENSO event develops and matures, and Year 1 as the following year.

We find that the composite SPOI is strongly positive for MY El Niño, reaching 0.89 standard deviations (s.d.), but remains near zero for SY El Niño at −0.26 s.d., indicating a clear difference (Fig. 1a). During La Niña, this contrast becomes even more pronounced, with the SPOI strongly negative at −0.68 s.d. during MY La Niña, while notably positive at 0.63 s.d. during SY La Niña (Fig. 1b). The differences in the SPOI between MY and SY ENSO events are statistically significant at the 95% confidence level for both El Niño and La Niña. The seasonal evolutions of the composite SPOI (Fig. 1c, d) show that these differences persist through the boreal winters of Year 0 and Year 1. However, no significant differences are detected during the spring of Year 0.

We also analyzed the composite SLP anomalies during FMA[1] for MY and SY El Niño and La Niña events (Fig. 1e–h) and found that all MY ENSO composites exhibit a clear resemblance to the SPO pattern (Supplementary Fig. 1). The composite SLP anomaly structure for MY El Niño closely aligns with the positive SPO phase, showing a strong pattern correlation of 0.80 ($p < 0.01$; Fig. 1e). In contrast, the SLP anomaly pattern for SY El Niño does not display a distinct SPO signature (Fig. 1f), with only a weak spatial correlation ($R = −0.13$, $p > 0.2$). Similarly, the SLP pattern associated with MY La Niña is characterized by a negative SPO phase (Fig. 1g), with a high spatial correlation of −0.84 ($p < 0.01$), whereas SY La Niña lacks this negative SPO pattern entirely (Fig. 1h). These results highlight the presence

of a robust SPO signal in MY ENSO events, while such a signal is notably absent in SY ENSO events.

In this study, MY ENSO events were defined using a relatively lenient second-year criterion, requiring only that the Niño3.4 index maintain the same sign as the first year, without needing to exceed the ENSO threshold (see Methods and Supplementary Table 1)[2,44,45]. For validation, a stricter criterion (second-year Niño3.4 > 0.5 s.d.) was also tested, and the SPO differences between MY and SY ENSO events remained robust (Supplementary Table 2). However, this stricter definition reduced MY El Niño samples to just five, limiting statistical confidence. The more flexible criterion ultimately provided a larger sample size and improved statistical robustness.

To overcome the limited sample sizes of observed MY and SY ENSO events, we examined 165-year historical simulations (1850–2014) from 45 CMIP6 models (Supplementary Table 3) to evaluate the robustness of SPO differences. Most models consistently simulate a positive SPOI for MY El Niño (82%, 37 out of 45 models; Fig. 2a) and a negative SPOI for MY La Niña (89%, 40 out of 45 models; Fig. 2c). In contrast, no consistent SPOI signal emerges for SY ENSO events, with values fluctuating around zero (Fig. 2b, d). The multi-model ensemble mean (MME) further highlights this contrast: MY El Niño and La Niña show significant positive and negative SPOI (0.16 and −0.19 s.d.), respectively, while SY events show near-zero SPOI (−0.04 and 0.01 s.d.). These model results confirm the key observational finding that the SPO is a distinguishing feature of MY ENSO events. They also demonstrate that CMIP6 models can reasonably capture this important difference between MY and SY ENSO.

Mechanisms for different SPO conditions under MY and SY ENSOs

Previous studies have revealed that SPO can be forced by tropical Pacific SST variations[35]. Therefore, the differing SPO conditions between MY and SY ENSO events may be linked to differences in their tropical Pacific SSTA patterns. Fig. 3a–d show the composite SSTA patterns for different types of ENSO during FMA[1] based on observations. For El Niño (Fig. 3a, c), the SSTAs in the MY El Niño have a more westward central location than SY El Niño (159.4°W vs. 151.4°W; see Methods for definition), while SSTA intensities are comparable with similar Cold Tongue Index (CTI) value (0.58 °C vs. 0.57 °C). For La Niña (Fig. 3b, d), the MY La Niña displays a much stronger magnitude (−0.65 °C) than the SY La Niña (−0.22 °C) and a more westward central location (162.6°W vs. 155.9°W).

To examine the possible impact of ENSO intensity on the occurrence of the SPO, we examine in Fig. 3e, f the linear linkage between the ENSO intensity (CTI) and SPOI. A notable correlation is found for La Niña, where stronger La Niña events are associated with more pronounced negative SPO, while moderate La Niña events are linked to neutral or even positive SPO ($R = 0.63$, $p < 0.01$; Fig. 3f). In contrast, this correlation is weak for El Niño, showing no clear trend that stronger El Niño events may correspond to stronger positive SPO ($R = −0.06$; Fig. 3e). This contrasting strong influence of La Niña intensity to SPO and weak influence of El Niño intensity to SPO remain consistent across various ENSO intensity indices (see results of Niño3.4, Niño3, and Niño4 indices in Supplementary Table 4).

Next, we assess the potential influence of ENSO location on SPO occurrence by examining the relationship between ENSO zonal location (see Methods for definition) and SPOI (Fig. 3g, h). For El Niño, we find a moderate negative correlation ($R = −0.30$), suggesting that more westward events are more likely to trigger a positive SPO, though this correlation does not reach the 90% confidence level ($p < 0.2$). In contrast, La Niña shows almost no relationship between zonal location and SPO ($R = −0.07$). Notably, all MY El Niño events occur when the central SSTA is located west of 125°W.

In general, La Niña events tend to be centered over the central equatorial Pacific, while El Niño events can occur across both the central and eastern equatorial Pacific (Fig. 3g, h). Consequently, El Niño events are typically categorized into EP and CP types[27,28]. The reason the SPO responds to El Niño varies with its type, specifically the central location of the El Niño's SST anomalies, is that El Niño events must trigger deep convection to
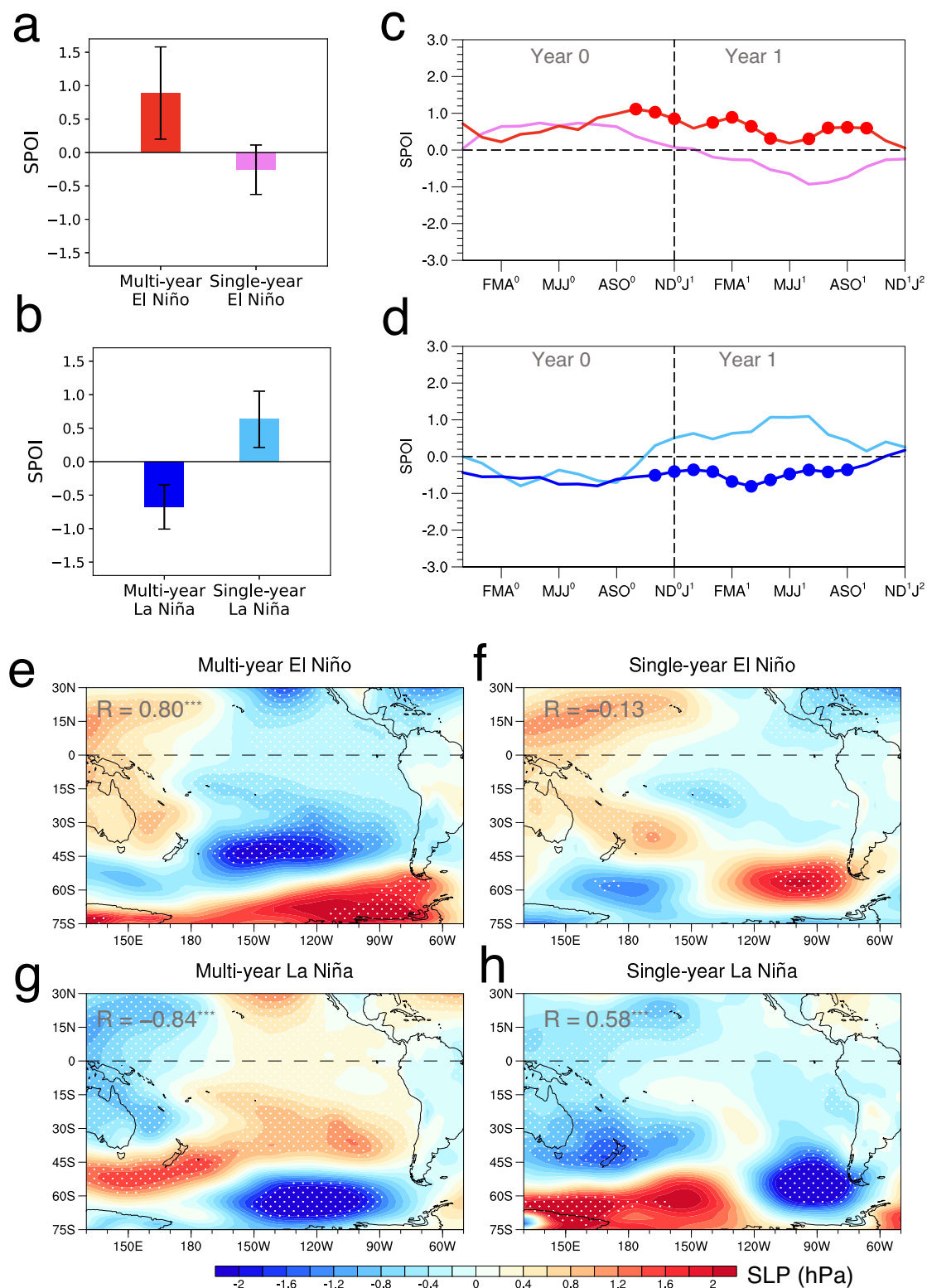
Fig. 1 | Comparison of South Pacific Oscillation between multi-year and single-year ENSO events. a Composite SPO indices for MY and SY El Niño events in FMA[1] from 1950 to 2023, and b for MY and SY La Niña events, with error bars indicating the 95% confidence intervals. c Composite monthly SPO indices for MY (red line) and SY (pink line) El Niño events, and d for MY (blue line) and SY (azure line) La Niña events. c, d The evolution of the SPO indices from the first year to the second year of the ENSO lifecycle. All SPO indices are smoothed using a 3-month window and standardized for each calendar month. Dots over the line of MY ENSO represent months where the differences in SPO indices between MY and SY ENSO events are significant at the 95% confidence level. Composite SPO spatial patterns (shading; hPa) in FMA[1] for e MY El Niño, f SY El Niño, g MY La Niña, and h SY La Niña. White dots represent the SLP anomalies that are significant at the 95% confidence level. Spatial correlation coefficients (R) between SLP anomalies over the South Pacific (75°S–0°, 180°–90°W) and the typical SPO pattern (Supplementary Fig. 1) are shown in the upper left corner of each panel. Three asterisks indicate that the correlation coefficients have passed the 99% confidence test.
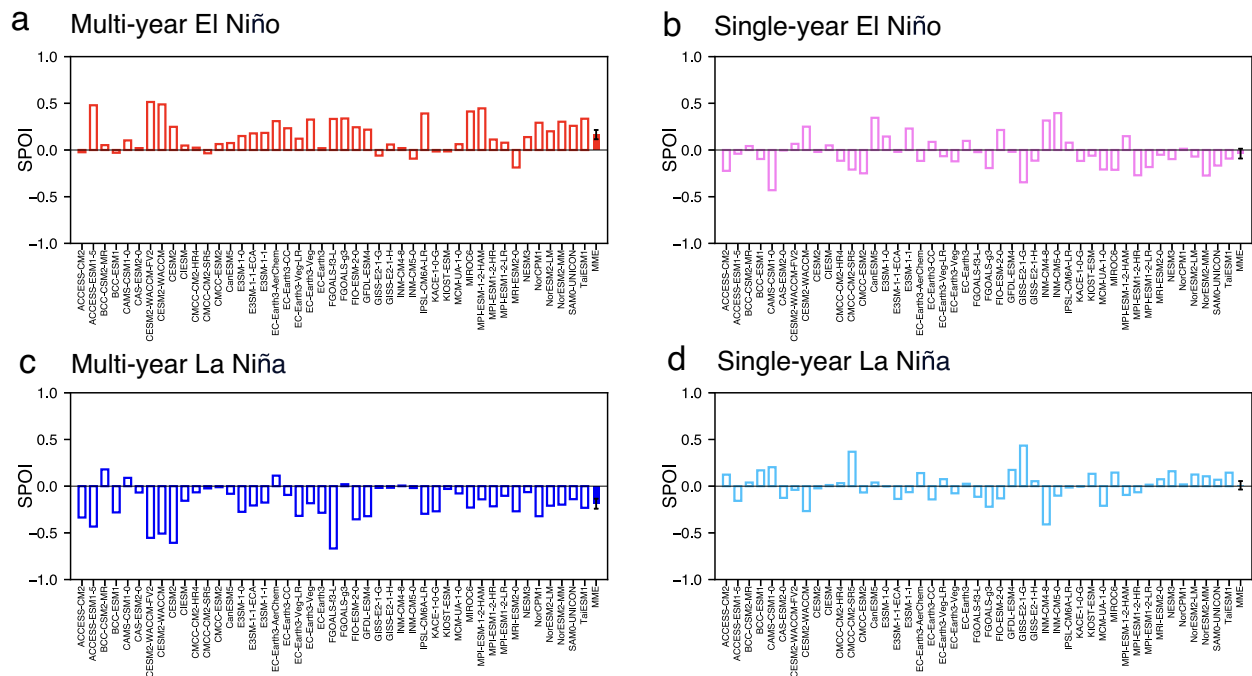
Fig. 2 | Composite SPO indices for multi-year and single-year ENSO events across CMIP6 models. The mean SPO indices for each CMIP6 model (hollow bars) are presented for **a** MY El Niño, **b** SY El Niño, **c** MY La Niña, and **d** SY La Niña during the second-year boreal spring. The solid bars on the far right of each subplot represent the ensemble mean of 45 models. Error bars indicate the 95% confidence interval.

produce a teleconnection to the Southern Hemisphere, which gives rise to the SPO. Background SSTs in the central equatorial Pacific often exceed 27.5 °C (Supplementary Fig. 2), the threshold necessary to initiate deep convection. Therefore, SST anomalies associated with CP El Niño events can easily excite anomalous deep convection, facilitating the development of the SPO. In contrast, the background SSTs in the eastern equatorial Pacific are generally well below the 27.5 °C threshold. As a result, even strong warming associated with EP El Niño events is less effective at triggering deep convection, and thus less capable of inducing the SPO teleconnection.

The dependence of the SPO response on the location of El Niño warming is clearly illustrated in Supplementary Fig. 3, which compares SLP anomalies in the South Pacific during CP and EP El Niño events. During CP El Niño events, strong negative SLP anomalies dominate the SPO region and extend westward to 180°W. In contrast, EP El Niño events exhibit weaker negative SLP anomalies, with the anomaly center confined east of 150°W. Supplementary Fig. 4 further demonstrates that even the three strongest EP El Niño events (1982/83, 1997/98, and 2015/16) fail to generate a significant SPO response. As for CP El Niño events, Fang and Yu[24] found that once the SST exceeds the 27.5 °C threshold for deep convection, further increases in SST anomaly amplitude do not substantially enhance convective activity. Together, these results explain why the longitudinal location of El Niño warming is more critical than its intensity in driving the development of the SPO.

In contrast, La Niña events are almost exclusively centered in the central equatorial Pacific (Fig. 3h). In this region, background SSTs are typically just above the threshold required to initiate deep convection. Strong negative SST anomalies during intense CP La Niña events can lower local SSTs below this threshold, completely suppressing deep convection. This suppression leads to substantial changes in latent heat flux, which in turn generates significant atmospheric teleconnections to the South Pacific and gives rise to a strong SPO response. Conversely, weaker CP La Niña events do not reduce SSTs enough to inhibit deep convection, resulting in smaller heat flux changes and a weaker SPO response. Thus, for La Niña events, the magnitude of the SST anomalies plays a key role in determining the strength of the SPO response.

The above observational analyses indicate that the central location of El Niño and the intensity of La Niña are key factors in shaping SPO responses during boreal winter following the first-year ENSO peak. To further validate the controlling role of ENSO's location and magnitude on SPO formation, we conducted a 30-member ensemble experiment using the Geophysical Fluid Dynamics Laboratory Atmospheric Model version 2.1 (GFDL AM2.1) model[46]. The model was forced by observed monthly SSTAs from 1951 to 2018 within the tropical Pacific domain (20°S–20°N, 140°E–90°W, with a 5° inner buffer zone), while maintaining climatological SSTs elsewhere (see Methods for details). We focused on evaluating the simulated SPO responses during prescribed MY and SY ENSO events (Supplementary Table 1). To isolate the ENSO forcing, we examined the 30-member ensemble mean of the simulated SPOI (Fig. 4a, b). Consistent with observations, MY El Niño events forced a stronger positive SPO than SY El Niño events, while MY La Niña events forced a stronger negative SPO than SY La Niña events.

However, a notable discrepancy between observations and the forced atmospheric model experiment emerged. In the simulations, SPOI in SY ENSO events retains the same sign as in MY ENSO events and remains significantly different from zero (Fig. 4a, b). In contrast, observations show that SPOI in SY ENSO events differs substantially from that in MY ENSO events, even exhibiting opposite signs (Fig. 1a, b). This discrepancy suggests that internal atmospheric variability, largely reduced or removed in the 30-member ensemble mean, may be playing a role in modulating the ENSO-forced SPO in observations. This effect is particularly pronounced in SY El Niño and SY La Niña events, where the weaker ENSO-forced SPO allows internal variability to drive substantial deviations, bringing the values closer to those observed. It should be noted that the discrepancy between observations and the forced atmospheric model results may also be influenced by model dependence, and further studies using multiple AGCMs would help to assess the robustness of our findings.

To assess the influence of internal variability, we examined the spread of SPOI across the 30-member ensemble for each historical ENSO event (Fig. 4c–f). For most events (45 out of 51), the observed SPOI falls within the ensemble spread, indicating that observed SPO variance can largely be explained by ENSO forcing combined with internal atmospheric variability.
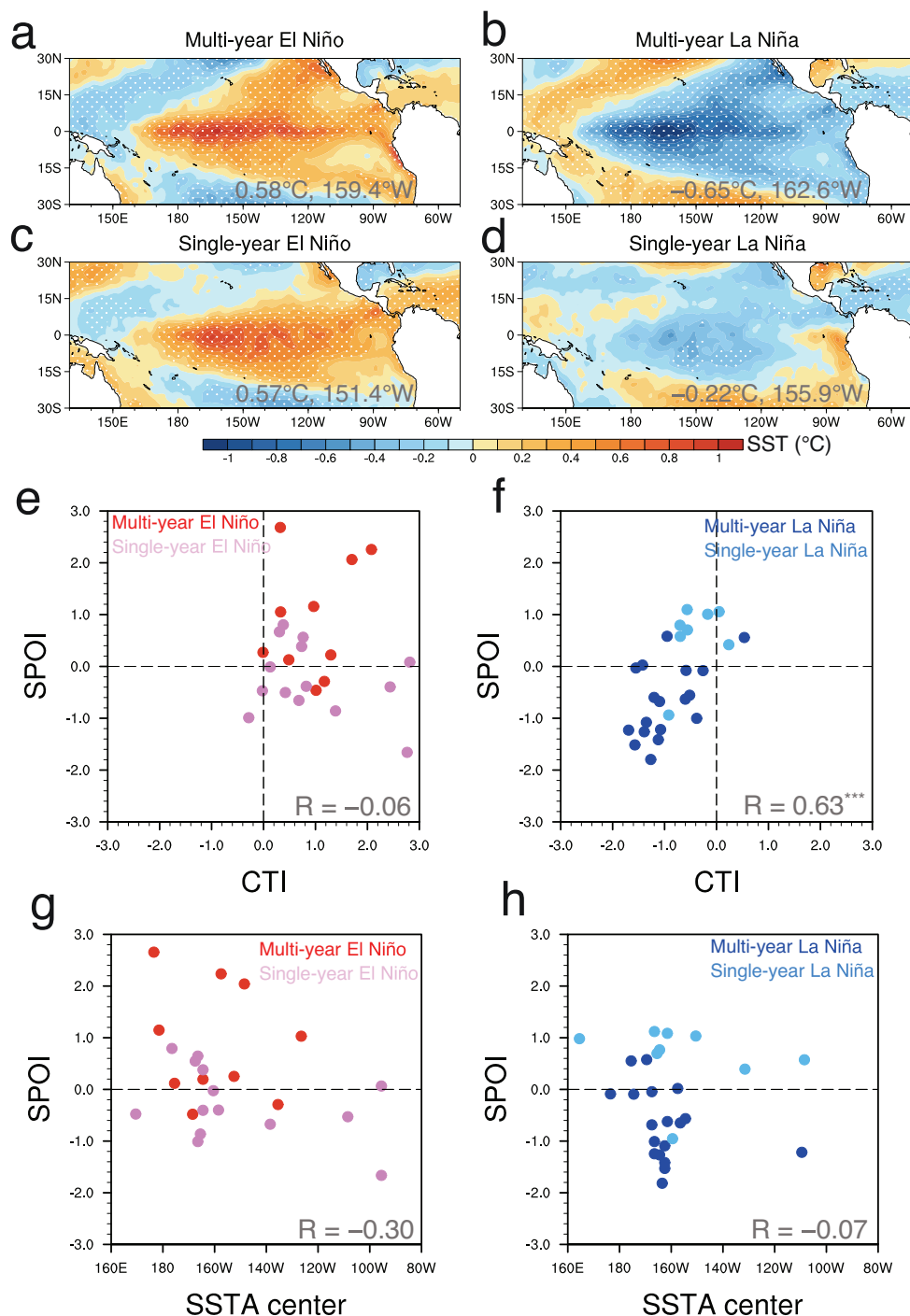
Fig. 3 | Linkages between the SPO and simultaneous ENSO properties. Composite SST anomalies (shading; °C) are shown for **a** MY El Niño, **b** SY El Niño, **c** MY La Niña, and **d** SY La Niña during FMA[1]. The CTI strength and the equatorial longitudinal location of maximum (minimum) SST anomalies are indicated in each panel. Scatter plots of the SPOI versus **e** CTI for El Niño, **f** CTI for La Niña, **g** SSTA center for El Niño, and **h** SSTA center for La Niña. In (**e–h**), red (pink) dots represent MY (SY) El Niño, and blue (azure) dots represent MY (SY) La Niña. Correlation coefficients (R) between the CTI (or SSTA center) and SPOI are indicated in each panel, with three asterisks denoting that the correlation coefficients have passed the 99% confidence test.

Notably, for SY El Niño events, observed SPOI tends to cluster near the lower edge of the ensemble spread (Fig. 4d), while for SY La Niña events, it tends to sit near the upper edge (Fig. 4f). In contrast, MY El Niño and La Niña events show no such systematic bias (Fig. 4c, e). Among 14 SY El Niño events, 8 have observed SPOI below the 75th percentile, suggesting internal variability may weaken the simulated positive SPO response (Fig. 4a), shifting it toward the observed negative SPO (Fig. 1a). Similarly, for 9 SY La Niña events, 6 show observed SPOI above the 25th percentile, implying

internal variability could shift the simulated negative SPOI (Fig. 4b) toward the observed positive SPOI (Fig. 1b). These results suggest internal atmospheric variability plays a larger role in shaping SPO for SY ENSO events compared to MY ENSO events.

Taken together, these findings suggest that ENSO characteristics initially determine the relative strength of the SPO. Subsequently, atmospheric internal variability plays a role. When ENSO forcing is weak, internal variability is more likely to diminish the ENSO-forced SPO to near
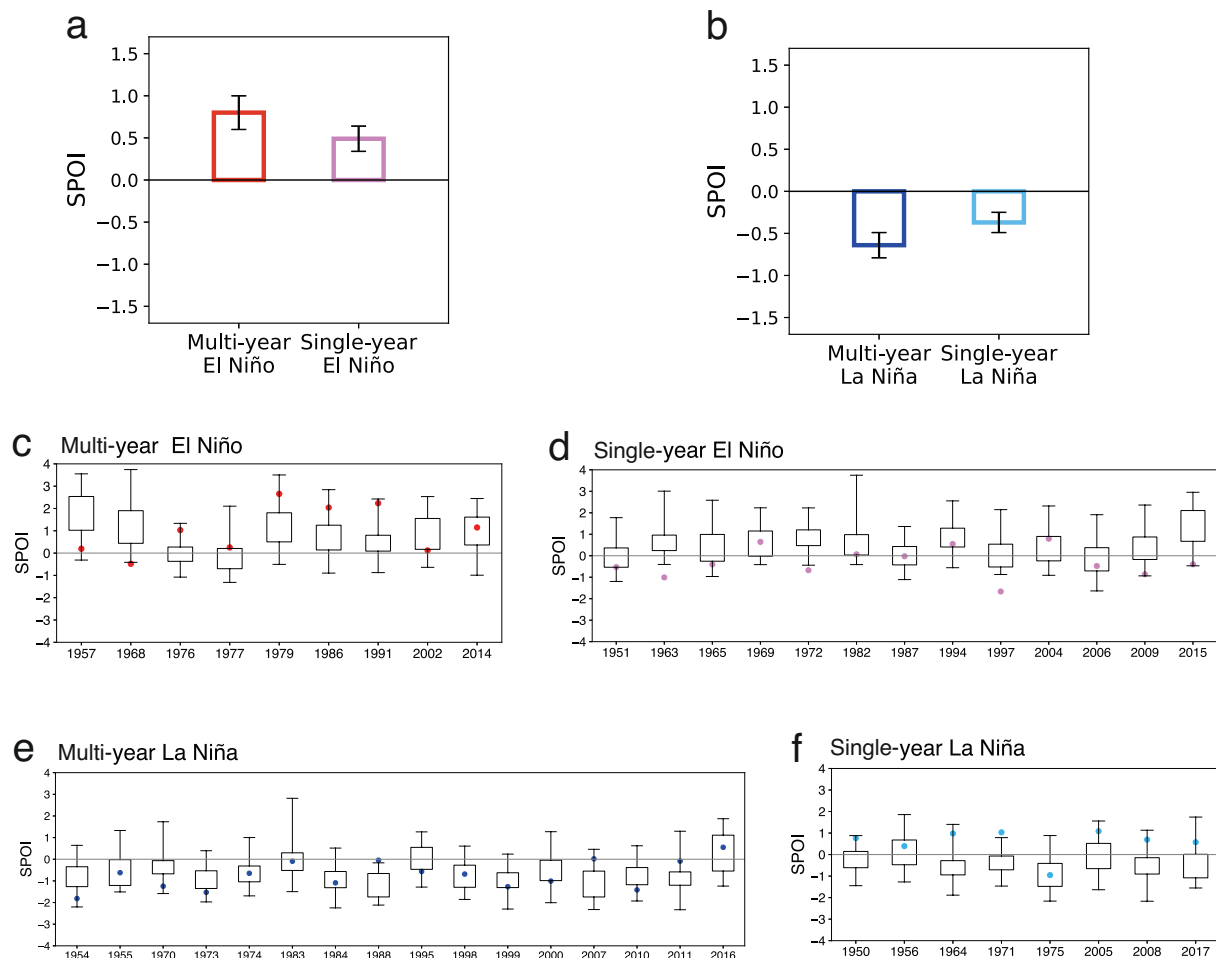
Fig. 4 | Simulated responses of the SPO to ENSO events in the forced AGCM experiments. The model experiments were conducted using prescribed monthly varying SST anomalies over the tropical Pacific (20°S–20°N, 140°E–90°W). **a, b** The 30-member ensemble mean SPOI during the second-year boreal spring for composite MY El Niño (red bar) and SY El Niño (pink bar), and for MY La Niña (blue bar) and SY La Niña (azure bar) events, respectively. Error bars indicate the 95% confidence interval. Box plots of simulated SPOI distributions for individual events, including **c** 10 MY El Niño events, **d** 14 SY El Niño events, **e** 18 MY La Niña events, and **f** 9 SY La Niña events. Each boxplot represents the distribution across the 30 ensemble members. Colored dots overlaid on the box plots indicate observed SPOI values for reference. The whiskers denote the maximum and minimum values, while the box boundaries correspond to the interquartile range (25th–75th percentiles) of the simulated SPOI. Years on the *x*-axis indicate the first developing year of each ENSO event.

zero or even reverse its phase. Conversely, when ENSO forcing is strong (due to high intensity or a more westward-located central ENSO SST anomalies), the ENSO-forced SPO response can maintain a relatively strong level even when affected by internal variability.

Feedback from the South Pacific on different ENSO evolutions
In this section, we further explore how the SPO, shaped by the combined effects of first-year ENSO forcing and atmospheric internal variability, feedbacks to the tropical Pacific and influences the evolution of second-year ENSO. To investigate the feedback processes, we examined the evolution of SST and 10 m horizontal wind anomalies, composited for MY and SY ENSO events, from FMA[1] to ND[1]J[2] (November–January) in observation (Supplementary Figs. 5 and 6).

During FMA[1], the Southwest Pacific exhibits southerly surface wind anomalies associated with the strong positive SPO in MY El Niño (about 0.5 m/s; Fig. 5a). Given that the climatological 10 m wind over the Southwest Pacific is southeasterly (Supplementary Fig. 7), the positive SPO-induced southerly anomalies enhance the climatological winds, increasing local evaporation and cooling SSTs. This leads to a gradual cooling in the Southwest Pacific during MY El Niño (Fig. 5a). This cooling sustains from FMA[1] through ND[1]J[2] (Fig. 5a) and spreads toward the equatorial far-

western Pacific via the WES mechanism, strengthening SSTA cooling there (Supplementary Fig. 5a). In SY El Niño, the weak anomalous southerly during FMA[1] shifts to northerly during MJJ[1] (March–July; −0.21 m/s) (Fig. 5a), causing warm SST anomalies to develop due to the weakening of the climatological southerlies (Fig. 5a and Supplementary Fig. 5b). These warm SST anomalies intensify through MJJ[1], ASO[1] (August–October), and ND[1]J[2] (Fig. 5a).

In the Southeast Pacific, westerly wind anomalies appear during FMA[1] in MY El Niño (about 0.26 m/s), accompanied by warm SST anomalies (Fig. 5b). Due to the background southeasterly (Supplementary Fig. 7), these westerly winds and warm SSTAs reinforce each other through the WES feedback, maintaining the warm SSTAs and driving them toward the tropics in the subsequent seasons (Fig. 5b and Supplementary Fig. 5a). In SY El Niño, negative SPO-related strong easterly and southerly winds take over in MJJ[1], resulting in localized cold SSTAs that develop toward the equator (Fig. 5b and Supplementary Fig. 5b).

Combining the SPO-induced impacts over the western and eastern Pacific, we find that during MY El Niño, colder SSTs in the far-western Pacific and warmer SSTs in the eastern Pacific—both driven by the positive SPO—create a positive SST gradient across the tropical Pacific, enhancing equatorial westerly winds (Supplementary Fig. 5a). These westerly winds
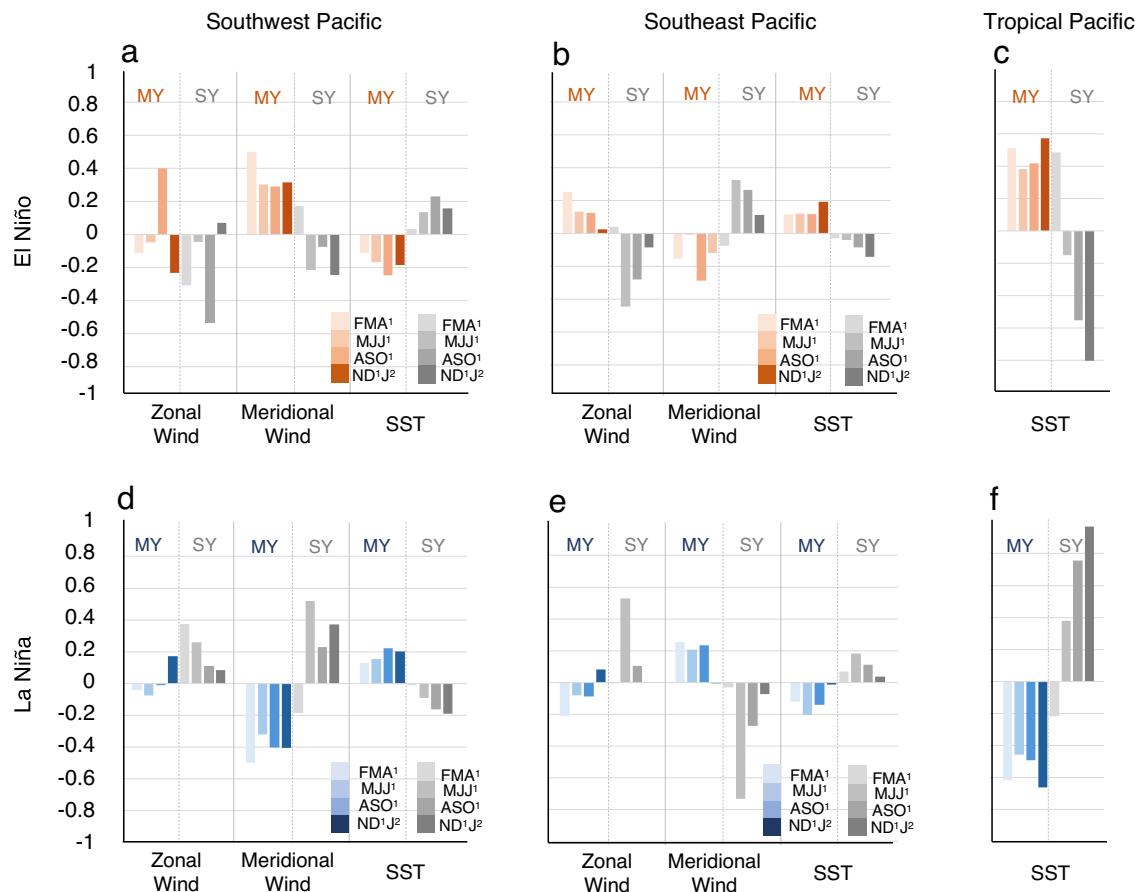
Fig. 5 | Quantitative examination of the feedback from the SPO to subsequent ENSO events. a–c Seasonal evolutions of regional mean values for 10 m zonal wind (m/s), meridional wind (m/s), and SST anomalies (°C) in MY El Niño (orange bars) and SY El Niño (gray bars). Values are averaged over **a** Southwest Pacific (15°S–35°S, 160°E–170°W), **b** Southeast Pacific (15°S–35°S, 76°W–103°W), and **c** Tropical Pacific (CTI) regions. Progressively darker shades correspond to seasons FMA[1], MJJ[1], ASO[1], and ND[1]J[2], respectively. **d–f** The same variables as in (**a–c**), but for La Niña events, comparing MY (blue bars) and SY (gray bars).

cause a lowering of the thermocline in the eastern equatorial Pacific through eastward-propagating Kelvin waves, which help further develop warm SSTs in the east-central Pacific. The CTI remains positive and continues to strengthen from MJJ[1] through ND[1]J[2] (Fig. 5c), contributing to the first-year El Niño becoming an MY event. In contrast, for SY El Niño, warm SSTs in the western Pacific and cold SSTs in the eastern Pacific generate a negative SST gradient, weakening the residual equatorial westerly winds from the previous year's El Niño. This reversal shifts the first-year CTI from a warm phase in FMA[1] to a cold phase in MJJ[1], ASO[1], and ND[1]J[2] (Fig. 5c). Thus, the absence of a positive SPO prevents the warm SSTs of the first-year SY El Niño from sustaining into the second year, leading to a failure to produce consecutive El Niño events.

A similar but opposite evolution occurs for SY and MY La Niña events (Fig. 5d–f and Supplementary Fig. 6). The bars shown in Fig. 5d–f for MY and SY La Niña events are generally reversed compared to the bars shown in Fig. 5a–c for MY and SY El Niño events. In brief, the negative SPO during MY La Niña leads to warm SSTAs in the tropical western Pacific and cold SSTAs in the tropical eastern Pacific, forming a negative zonal SST gradient that sustains equatorial easterly winds, maintaining the event as a MY La Niña (Supplementary Fig. 6a). In SY La Niña, the opposite occurs (Supplementary Fig. 6b). As a result, the absence of a negative SPO in SY La Niña prevents the cold SSTs from persisting into the second year, thus inhibiting the formation of consecutive La Niña events.

It is worth noting that several previous studies have shown that a positive SPO tends to induce SST warming in the tropical Pacific, while a negative SPO often leads to cooling[35,37,38]. Those studies conducted coupled climate model experiments to investigate extratropical–tropical interactions

by prescribing SPO-related SST anomalies and analyzing the resulting response in the tropical Pacific. Therefore, we do not repeat similar numerical experiments in this study to reconfirm these interaction mechanisms. However, it is important to highlight that these modeling studies did not address the potential influence of the SPO on the evolution of SY and MY ENSO events. This aspect is the central focus of the present study, in which we examine the feedback role of the SPO following the first year of ENSO development.

Enhanced predictability of MY ENSO via the SPO

ENSO's prediction skills exhibit seasonal variations, with a strong spring predictability barrier (SPB)[47–50], which means the lowest prediction skill for the prediction implemented starts from the boreal spring season. The SPO precursor we employed in this study is in the boreal spring season, which may potentially reduce SPB and enhance ENSO predictability.

Therefore, we conducted a predictability assessment by comparing the SPO-based forecast approach with the operational ENSO forecast provided by the International Research Institute for Climate and Society (IRI). Since the earliest available IRI forecast begins in 2002, we limited our comparison to ENSO events occurring after that year. For the IRI forecasts, we focused on those issued in April and targeting the NDJ season of the decaying year of ENSO events. After an El Niño, if the IRI forecast assigned more than a 50% probability to another El Niño occurring, we classified it as a forecast of a MY El Niño event; otherwise, it was considered a forecast of a SY El Niño event. The same criteria were applied to La Niña cases. For the SPO-based forecast, we used the SPO index from the FMA season. If the SPO index was greater than zero after an El Niño, we forecast a MY El Niño event; if less

Article

than zero, a SY El Niño. Similarly, after a La Niña, a negative SPO index forecasted a MY La Niña event, while a positive index indicated a SY La Niña.

The forecast accuracies are summarized in Supplementary Tables 5–8. The IRI forecast correctly predicted: 2 out of 3 MY El Niño events (67%), 1 out of 6 MY La Niña events (17%), 3 out of 5 SY El Niño events (60%), and 3 out of 4 SY La Niña (75%). In summary, SY La Niña events had the highest predictability (75%), followed by MY El Niño (67%), SY El Niño (60%), and the most challenging one, MY La Niña (17%). Comparing across ENSO phases, MY and SY El Niño events exhibited comparable predictability (67% vs. 60%), but MY La Niña events were significantly harder to forecast than SY La Niña (17% vs. 75%). Overall, MY ENSO events were forecast with much lower accuracy than SY ENSO events (33% vs. 67%). Given the increasing occurrence of MY La Niña events in recent years and projected into the future[1–3], improving the prediction skill for MY ENSO, especially the MY La Niña, is particularly urgent.

We then evaluated the prediction skill of the MY and SY ENSO events using the SPO precursor. The SPO-based method correctly forecasted: 2 out of 3 MY El Niño events (67%), 3 out of 6 MY La Niña events (50%), 3 out of 5 SY El Niño events (60%), and 4 out of 4 SY La Niña events (100%). Notably, the SPO precursor substantially improved the forecast accuracy for MY La Niña events (50% vs. 17% from IRI), while maintaining similar performance in the other categories. This indicates that the SPO index offers a simple and effective tool for enhancing ENSO prediction skill where it is most needed. We further extended the SPO forecast analysis to the full 1950–2023 period. The results were as follows: 8 out of 10 MY El Niño (80%), 14 out of 18 MY La Niña (78%), 9 out of 14 SY El Niño (64%), and 8 out of 9 SY La Niña (89%) were correctly forecasted using the SPO-based method. With this larger sample, the SPO-based forecasts exhibited even higher skill, especially for MY events: (El Niño: 80%; La Niña: 78%). This suggests possible interdecadal variations in the SPO–ENSO relationship. While this warrants further investigation, such analysis is beyond the scope of the present study. Overall, the SPO precursor achieved an impressive 79% accuracy for forecasting MY ENSO events, underscoring its strong potential in operational seasonal prediction.

Summary and discussions
The SPO plays a crucial role in distinguishing between SY and MY ENSO events, with significant positive (negative) SPO anomalies linked to MY El Niño (La Niña) events, while SY El Niño (La Niña) events are associated with the absence of such anomalies. This relationship, observed in both reanalysis data and CMIP6 simulations, is driven by first-year ENSO properties, including the longitudinal location of El Niño and the intensity of La Niña, with South Pacific atmospheric internal variability further modulating the SPO response. Unlike previous studies that primarily focus on one phase of ENSO, explaining why La Niña tends to persist over multiple years[51,52], the SPO proxy used in this study is applicable to both El Niño and La Niña phases and can be regarded as a unified mechanism for MY ENSO. Compared to the forecast skill of dynamical and statistical models from IRI, our SPO-based approach shows enhanced ENSO forecast skill, especially in MY La Niña. These findings have significant implications for our understanding of MY ENSO dynamics and prediction.

Besides the SPO, other climate modes in the South Pacific, like the Southern Annular Mode[53,54], the Pacific-South American Mode[55], the South Pacific Quadrupole Mode[33], and the SPMM, may also play roles in differentiating MY and SY ENSO, and could be further investigated in future research. In addition, given the significant contribution of South Pacific air-sea variability to the recent 2020–2023 triple-dip La Niña event[5–7], it is possible that the SPO–ENSO relationship has undergone decadal variations. Therefore, it is worthwhile to examine the decadal evolution of the SPO–ENSO relationship, its potential connection to the South Pacific Decadal Oscillation[56,57] or the Pacific Decadal Oscillation[58], and its future projection under climate change. While this is an important direction for future research, such an analysis is beyond the scope of the present study.

This study highlights the important role of extratropical Southern Hemisphere processes in shaping MY ENSO evolution, a factor that has been less emphasized compared to influences from other basins. It is important to note that the highlighted role of South Pacific climate variability in distinguishing MY and SY ENSO does not preclude contributions from other regions, including the tropical Pacific, North Pacific, Atlantic, and Indian Ocean[23,59–65]. In fact, certain ENSO events, such as those in 1968/69, 1975/76, 2004/05, and 2016/17, cannot be fully explained by South Pacific processes alone (Fig. 4c–f). Future studies should examine the combined and potentially interactive roles of these basins in modulating ENSO evolution.

Methods
Reanalysis data
This study utilized global monthly SST data from the Hadley Centre Global Sea Ice and Sea Surface Temperature dataset (HadISST), which has a horizontal resolution of 1° × 1°[66]. SLP data and horizontal 10 m wind data were sourced from the National Centers for Environmental Prediction-National Center for Atmospheric Research reanalysis 1 (NCEP/NCAR R1) dataset with a resolution of 2.5° × 2.5°[67]. The analysis spans the period from 1950 to 2023. To mitigate the influence of global warming, long-term linear trends were removed from the data prior to analysis. Monthly anomalies were computed by subtracting the climatological monthly means calculated over the entire analysis period.

CMIP6 historical outputs
To evaluate the distinct influence of the SPO on MY and SY ENSO, we employed CMIP6 models[68]. Monthly historical simulations, specifically SST and SLP variables, were utilized from 45 different CMIP6 models (Supplementary Table 3). The analysis covered the same period across all 45 models, spanning 165 years from 1850 to 2014. This comprehensive dataset allows for a robust assessment of the SPO's role in different ENSO types across a range of climate models.

Definitions of climate indices
The SPO index was defined as the reversed average of SLP anomalies over the region 46°S–27°S and 165°E–82°W, both in observation and modeling[35,38]. Therefore, the positive phase of the SPO corresponds to negative SLP anomalies over the subtropical South Pacific (Supplementary Fig. 1). To quantify the strength of ENSO, several Niño indices were employed, each defined as the SSTAs averaged across various specific regions of the tropical Pacific: CTI (6°S–6°N and 180°–90°W), Niño3.4 index (5°S–5°N and 170°–120°W), Niño3 index (5°S–5°N and 150°W–90°W), and Niño4 index (5°S–5°N and 160°E–150°W). Longitudinal location of El Niño (La Niña) was determined as the longitude of the maximum (minimum) SST anomalies, after computing the 5°S–5°N meridional mean and applying a 10-degree zonally running mean.

Identified MY and SY ENSO events
We employed a commonly used definition to identify ENSO events and their different evolution types[2,44,45]. An El Niño (La Niña) event was identified when the NDJ running-mean Niño3.4 index exceeded 0.5 (−0.5) s.d. Applying this criterion, we identified a total of 24 El Niño and 27 La Niña events (Supplementary Table 1) from 1950 to 2023. Further classification into MY or SY ENSO types was based on the Niño3.4 index during the second-year winter. ENSO events were categorized as MY El Niño (La Niña) if the second-year NDJ[1] Niño3.4 index was greater (less) than zero, and SY El Niño (La Niña) if it was less (greater) than zero[2,44,45]. We adopted this relatively loose criterion for two primary reasons. Firstly, this criterion serves to augment the pool of samples available for analysis, a crucial factor given the scarcity of MY ENSO events. Secondly, our study primarily aims to unveil the diverse underlying physical processes influencing the persistence or diminution of SST warming/cooling during the second year of ENSO events. Notably, there is no inherent expectation that the physical mechanisms sustaining SSTA in the second year should necessarily lead to

warming exceeding a specific threshold (e.g., 0.5 s.d.). The classification patterns for all 51 identified El Niño and La Niña events are provided in Supplementary Table 1. The same criteria were applied for CMIP6 data to identify ENSO events and their different evolution types.

Identified CP and EP ENSO events

ENSO events are classified as CP or EP types based on the relative strength of the Niño4 and Niño1+2 indices. Th Niño4 index is defined as the SSTAs averaged over 5°S–5°N, 160°E–150°W, while the Niño1+2 index is defined over 10°S–0, 90°–80°W. An ENSO event is categorized as a CP (EP) type if the absolute value of the $ND^{0}J^{1}$ Niño4 index exceeds (is less than) that of the Niño1+2 index.

Climate model experiments

The atmospheric model employed in this study is the GFDL AM2.1[46]. This model features a horizontal resolution of 2.5° in longitude by 2° in latitude and consists of 24 vertical layers. For the experiment, we added historical monthly SSTAs (1951–2018) within the tropical Pacific domain (20°S–20°N and 140°E–90°W) to the modeled monthly varying climatological SSTs. Outside the tropical Pacific region, the model was forced solely by climatological SSTs. The experiment included 30 ensemble members, each initialized with slightly different disturbances and integrated for 68 years. This experiment design allows us to assess whether the SPO differences between MY and SY ENSO can be reproduced using ENSO-related tropical Pacific SST forcing alone.

Significance tests

The statistical significance of the composites and correlations was assessed using a two-tailed Student's t-test. The effective degrees of freedom (N_{eff}) were calculated based on the method proposed by Bretherton et al.[69]:

$$N_{eff} \approx N \frac{1 - r_x r_y}{1 + r_x r_y} \tag{1}$$

where N is the total number of samples, and r_x and r_y represent the lag-1 autocorrelations of variables x and y, respectively.

Data availability

All data utilized in this study are publicly accessible. The monthly SST data from the HadISST dataset can be obtained from https://www.metoffice.gov.uk/hadobs/hadisst/data/download.html. Monthly 10 m wind and SLP data from the NCEP/NCAR R1 are available at https://psl.noaa.gov/data/gridded/. The CMIP6 output dataset is accessible through the Earth System Grid Federation website: https://esgf-node.llnl.gov/projects/cmip6/. For access to the GFDL forcing experiment output, interested parties may contact the corresponding authors directly. The IRI-provided practical ENSO forecast is available at https://iri.columbia.edu/our-expertise/climate/forecasts/enso/.

Code availability

The data analysis in this study was conducted using NCAR Command Language (NCL; http://www.ncl.ucar.edu/) and Python (https://www.python.org/). All relevant code used for analysis and plotting is available upon request from the corresponding author.

References

1. Geng, T. et al. Increased occurrences of consecutive La Niña events under global warming. *Nature* **619**, 774–781 (2023).
2. Li, X., Yu, J.-Y. & Ding, R. El Niño-La Niña asymmetries in the changes of ENSO complexities and dynamics since 1990. *Geophys. Res. Lett.* **51**, e2023GL106395 (2024).
3. Wang, B. et al. Understanding the recent increase in multiyear La Niñas. *Nat. Clim. Change* 1–7. https://doi.org/10.1038/s41558-023-01801-6 (2023).
4. Allan, R. et al. The Context of the 2018–20 "Protracted" El Niño Episode: Australian drought and terrestrial, marine, and ecophysiological impacts. https://doi.org/10.1175/WCAS-D-22-0096.1 (2023).
5. Iwakiri, T. et al. Triple-Dip La Niña in 2020–23: North Pacific atmosphere drives 2nd year La Niña. *Geophys. Res. Lett.* **50**, e2023GL105763 (2023).
6. Li, X., Hu, Z.-Z., McPhaden, M. J., Zhu, C. & Liu, Y. Triple-Dip La Niñas in 1998–2001 and 2020–2023: impact of mean state changes. *J. Geophys. Res. Atmos.* **128**, e2023JD038843 (2023).
7. Shi, L., Ding, R., Hu, S., Li, X. & Li, J. Extratropical impacts on the 2020–2023 Triple-Dip La Niña event. *Atmos. Res.* **294**, 106937 (2023).
8. Timmermann, A. et al. El Niño–Southern Oscillation complexity. *Nature* **559**, 535–545 (2018).
9. Yu, J.-Y. & Fang, S.-W. The distinct contributions of the seasonal footprinting and charged-discharged mechanisms to ENSO complexity. *Geophys. Res. Lett.* **45**, 6611–6618 (2018).
10. Battisti, D. S. & Hirst, A. C. Interannual variability in a tropical atmosphere–ocean model: influence of the basic state, ocean geometry and nonlinearity. *J. Atmos. Sci.* **46**, 1687–1712 (1989).
11. Suarez, M. J. & Schopf, P. S. A delayed action Oscillator for ENSO. *J. Atmos. Sci.* **45**, 3283–3287 (1988).
12. Jin, F.-F. An equatorial ocean recharge paradigm for ENSO. Part I: conceptual model. *J. Atmos. Sci.* **54**, 811–829 (1997).
13. Jin, F.-F. An equatorial ocean recharge paradigm for ENSO. Part II: a stripped-down coupled model. *J. Atmos. Sci.* **54**, 830–847 (1997).
14. DiNezio, P. N. & Deser, C. Nonlinear controls on the persistence of La Niña. *J. Clim.* **27**, 7335–7355 (2014).
15. An, S.-I. & Kim, J.-W. Role of nonlinear ocean dynamic response to wind on the asymmetrical transition of El Niño and La Niña. *Geophys. Res. Lett.* **44**, 393–400 (2017).
16. Im, S.-H., An, S.-I., Kim, S. T. & Jin, F.-F. Feedback processes responsible for El Niño-La Niña amplitude asymmetry. *Geophys. Res. Lett.* **42**, 5556–5563 (2015).
17. Iwakiri, T. & Watanabe, M. Multiyear ENSO dynamics as revealed in observations, climate model simulations, and the linear recharge oscillator. *J. Clim.* **35**, 4025–4042 (2022).
18. Wu, X., Okumura, Y. M. & DiNezio, P. N. What controls the duration of El Niño and La Niña events? *J. Clim.* **32**, 5941–5965 (2019).
19. Wu, X., Okumura, Y. M., Deser, C. & DiNezio, P. N. Two-year dynamical predictions of ENSO event duration during 1954–2015. https://doi.org/10.1175/JCLI-D-20-0619.1 (2021).
20. Wu, X., Okumura, Y. M. & DiNezio, P. N. Predictability of El Niño duration based on the onset timing. *J. Clim.* **34**, 1351–1366 (2021).
21. Chiang, J. C. H. & Vimont, D. J. Analogous Pacific and Atlantic meridional modes of tropical atmosphere–ocean variability. *J. Clim.* **17**, 4143–4158 (2004).
22. Cai, W. et al. Pantropical climate interactions. *Science* **363**, eaav4236 (2019).
23. Ding, R. et al. Multi-year El Niño events tied to the North Pacific Oscillation. *Nat. Commun.* **13**, 3871 (2022).
24. Fang, S.-W. & Yu, J. A control of ENSO transition complexity by tropical Pacific mean SSTs through tropical-subtropical interaction. *Geophys. Res. Lett.* **47**, e2020GL087933 (2020).
25. Wang, C. Three-ocean interactions and climate variability: a review and perspective. *Clim. Dyn.* **53**, 5119–5136 (2019).
26. Zhao, S. et al. Explainable El Niño predictability from climate mode interactions. *Nature* **630**, 891–898 (2024).
27. Kao, H.-Y. & Yu, J.-Y. Contrasting eastern-Pacific and central-Pacific types of ENSO. *J. Clim.* **22**, 615–632 (2009).

28. Yu, J.-Y. & Kao, H.-Y. Decadal changes of ENSO persistence barrier in SST and ocean heat content indices: 1958–2001. *J. Geophys. Res. Atmos.* **112**, D13106 (2007).

29. Yu, J.-Y., Wang, X., Yang, S., Paek, H. & Chen, M. The changing El Niño–Southern Oscillation and associated climate extremes. in *Climate Extremes* 1–38. https://doi.org/10.1002/9781119068020.ch1 (American Geophysical Union (AGU), 2017).

30. Xie, S. & Philander, S. G. H. A coupled ocean-atmosphere model of relevance to the ITCZ in the eastern Pacific. *Tellus A* **46**, 340–350 (1994).

31. Kim, J.-W. & Yu, J.-Y. Understanding reintensified multiyear El Niño events. *Geophys. Res. Lett.* **47**, e2020GL087644 (2020).

32. Park, J.-H. et al. Mid-latitude leading double-dip La Niña. *Int. J. Climatol.* **41**, 1–18 (2020).

33. Ding, R., Li, J. & Tseng, Y. The impact of South Pacific extratropical forcing on ENSO and comparisons with the North Pacific. *Clim. Dyn.* **44**, 2017–2034 (2015).

34. Ding, R. et al. Relative contributions of North and South Pacific Sea surface temperature anomalies to ENSO. *J. Geophys. Res. Atmos.* **124**, 6222–6237 (2019).

35. Li, X., Ding, R., Tseng, Y.-H., Yu, J.-Y. & Xu, X. Mutual influences between ENSO and its two precursor modes in the extratropical South Pacific. *Clim. Dyn.* https://doi.org/10.1007/s00382-023-07054-5 (2024).

36. Li, X., Zhang, W., Ding, R. & Shi, L. Joint impact of North Pacific Victoria mode and South Pacific Quadrapole mode on Pacific ITCZ summer precipitation. *Clim. Dyn.* **54**, 4545–4561 (2020).

37. Min, Q. & Zhang, R. The contribution of Boreal Spring South Pacific atmospheric variability to El Niño occurrence. *J. Clim.* **33**, 8301–8313 (2020).

38. You, Y. & Furtado, J. C. The role of South Pacific atmospheric variability in the development of different types of ENSO. *Geophys. Res. Lett.* **44**, 7438–7446 (2017).

39. Zhang, H., Clement, A. & Di Nezio, P. The South Pacific meridional mode: a mechanism for ENSO-like variability. *J. Clim.* **27**, 769–783 (2014).

40. You, Y. & Furtado, J. C. The relationship between South Pacific atmospheric internal variability and ENSO in the North American multimodel ensemble phase-II models. *Geophys. Res. Lett.* **46**, 12398–12407 (2019).

41. Tseng, Y., Huang, J.-H. & Chen, H.-C. Improving the predictability of two types of ENSO by the characteristics of extratropical precursors. *Geophys. Res. Lett.* **49**, e2021GL097190 (2022).

42. Fang, X. et al. Will the historic southeasterly wind over the equatorial Pacific in March 2022 trigger a third-year La Niña event? *Adv. Atmos. Sci.* **40**, 6–13 (2023).

43. Song, C., Zhang, X., Zheng, F., Chen, X. & Jiang, H. The roles of off-equatorial subsurface cold-water incursions in triggering the second-year cooling of the La Niña event in 2021. *J. Mar. Sci. Eng.* **10**, 1667 (2022).

44. Kim, J.-W. & Yu, J.-Y. Single- and multi-year ENSO events controlled by pantropical climate interactions. *npj Clim. Atmos. Sci.* **5**, 1–11 (2022).

45. Lin, Y.-F. & Yu, J.-Y. The role of the Indian Ocean in controlling the formation of multiyear El Niños through subtropical ENSO dynamics. *J. Clim.* **37**, 385–401 (2024).

46. Delworth, T. L. et al. GFDL's CM2 global coupled climate models. Part I: formulation and simulation characteristics. *J. Clim.* **19**, 643–674 (2006).

47. Jin, E. K. et al. Current status of ENSO prediction skill in coupled ocean–atmosphere models. *Clim. Dyn.* **31**, 647–664 (2008).

48. Luo, J.-J., Masson, S., Behera, S. K. & Yamagata, T. Extended ENSO predictions using a fully coupled ocean–atmosphere Model. https://doi.org/10.1175/2007JCLI1412.1 (2008).

49. McPhaden, M. J. Tropical Pacific Ocean heat content variations and ENSO persistence barriers. *Geophys. Res. Lett.* **30**, 1480 (2003).

50. Webster, P. J. & Yang, S. Monsoon and ENSO: selectively interactive systems. *Q. J. R. Meteorol. Soc.* **118**, 877–926 (1992).

51. Liu, F. et al. New insights into multi-year La Niña dynamics from the perspective of a near-annual ocean process. *J. Clim.* **1**, 1–35 (2023).

52. Okumura, Y. M. & Deser, C. Asymmetry in the duration of El Niño and La Niña. *J. Clim.* **23**, 5826–5843 (2010).

53. Fogt, R. L. & Marshall, G. J. The Southern Annular Mode: variability, trends, and climate impacts across the Southern Hemisphere. *WIREs Clim. Change* **11**, e652 (2020).

54. Rogers, J. C. & van Loon, H. Spatial variability of sea level pressure and 500 mb height anomalies over the Southern hemisphere. https://doi.org/10.1175/1520-0493(1982)1102.0.CO;2 (1982).

55. Mo, K. C. Relationships between low-frequency variability in the southern hemisphere and sea surface temperature anomalies. *J. Clim.* **13**, 3599–3610 (2000).

56. Chen, X. & Wallace, J. M. ENSO-like variability: 1900–2013. https://doi.org/10.1175/JCLI-D-15-0322.1 (2015).

57. Lou, J., Holbrook, N. J. & O'Kane, T. J. South Pacific decadal climate variability and potential predictability https://doi.org/10.1175/JCLI-D-18-0249.1 (2019).

58. Newman, M. et al. The Pacific Decadal Oscillation, Revisited https://doi.org/10.1175/JCLI-D-15-0508.1 (2016).

59. Chen, S., Yu, B. & Chen, W. An analysis on the physical process of the influence of AO on ENSO. *Clim. Dyn.* **42**, 973–989 (2014).

60. Ham, Y.-G., Kug, J.-S. & Park, J.-Y. Two distinct roles of Atlantic SSTs in ENSO variability: North Tropical Atlantic SST and Atlantic Niño. *Geophys. Res. Lett.* **40**, 4012–4017 (2013).

61. Ham, Y.-G., Kug, J.-S., Park, J.-Y. & Jin, F.-F. Sea surface temperature in the north tropical Atlantic as a trigger for El Niño/Southern Oscillation events. *Nat. Geosci.* **6**, 112–116 (2013).

62. Izumo, T. et al. Influence of the state of the Indian Ocean Dipole on the following year's El Niño. *Nat. Geosci.* **3**, 168–172 (2010).

63. Jin, Y. et al. The Indian Ocean weakens the ENSO Spring predictability barrier: role of the Indian Ocean basin and dipole modes https://doi.org/10.1175/JCLI-D-22-0800.1 (2023).

64. Luo, J.-J., Liu, G., Hendon, H., Alves, O. & Yamagata, T. Inter-basin sources for two-year predictability of the multi-year La Niña event in 2010–2012. *Sci. Rep.* **7**, 2276 (2017).

65. Tokinaga, H., Richter, I. & Kosaka, Y. ENSO influence on the Atlantic Niño, revisited: multi-year versus single-year ENSO events. https://doi.org/10.1175/JCLI-D-18-0683.1 (2019).

66. Rayner, N. A. A. et al. Global analyses of sea surface temperature, sea ice, and night marine air temperature since the late nineteenth century. *J. Geophys. Res. Atmos.* **108**, 4407 (2003).

67. Kalnay, E. et al. The NCEP/NCAR 40-Year Reanalysis Project. *Bull. Am. Meteorol. Soc.* **77**, 437–472 (1996).

68. Eyring, V. et al. Overview of the Coupled Model Intercomparison Project Phase 6 (CMIP6) experimental design and organization. *Geosci. Model Dev.* **9**, 1937–1958 (2016).

69. Bretherton, C. S., Widmann, M., Dymnikov, V. P., Wallace, J. M. & Bladé, I. The effective number of spatial degrees of freedom of a time-varying field. https://doi.org/10.1175/1520-0442(1999)0122.0.CO;2 (1999).

Acknowledgements

Author contributions

X.M.L., J.Y.Y. and R.Q.D. designed the research. X.M.L. conducted the analyses and experiments. X.M.L. and J.Y.Y. drafted the manuscript, with

R.Q.D. providing revisions. X.F.X., K.J. and T.W. offered constructive suggestions for data analysis and manuscript improvement. All authors discussed the results and contributed feedback on the manuscript.

Competing interests

The authors declare no competing interests.

Additional information

Supplementary information The online version contains supplementary material available at https://doi.org/10.1038/s41612-025-01130-9.

Correspondence and requests for materials should be addressed to Jin-Yi Yu or Ruiqiang Ding.

Reprints and permissions information is available at http://www.nature.com/reprints

Publisher's note Springer Nature remains neutral with regard to jurisdictional claims in published maps and institutional affiliations.

1   Supplementary Information for:

2

3   **South Pacific Oscillation Contributes to Multi-year ENSOs**

4

5   Xumin Li[1,2,3], Jin-Yi Yu[1*], Ruiqiang Ding[2*], Xiaofeng Xu[3,4], Kai Ji[2], Tao Wen[2]

6

7   *[1]Department of Earth System Science, University of California, Irvine, CA 92697, USA*

8   *[2]Key Laboratory of Environmental Change and Natural Disasters of Chinese Ministry of*

9   *Education, Beijing Normal University, Beijing, China*

10 *[3]Key Laboratory of Meteorological Disaster of Ministry of Education (KLME), Nanjing University*

11 *of Information Science and Technology, Nanjing, China*

12 *[4]China Meteorological Administration Training Center, Beijing, China*

13

14   (*submitted to npj Climate and Atmospheric Science, first revision*)

15   *May 29, 2025*

16

17 ***** Corresponding author: Jin-Yi Yu (jyyu@uci.edu) and Ruiqiang Ding (drq@bnu.edu.cn)

18

19 This PDF file includes:

35 **Supplementary Figure 2.** Climatological SSTs over the tropical.

36 **Supplementary Figure 3.** Contrast in South Pacific SLP patterns between CP and EP

37 El Niño events.

38 **Supplementary Figure 4.** SLP anomaly patterns during three major EP El Niño events.

39 **Supplementary Figure 5.** Composite seasonal evolutions during the second-year of

40 multi-year and single-year El Niño.

41 **Supplementary Figure 6.** Composite seasonal evolutions during the second-year of

42 multi-year and single-year La Niña.

43 **Supplementary Figure 7.** Climatological horizontal wind over the South Pacific.

44 **Supplementary Table 1. Classification of multi-year and single-year ENSO events.**

45 The table categories MY El Niño, SY El Niño, MY La Niña, and SY La Niña events

46 from 1950 to 2023. The listed years refer to the first developing year of each ENSO

47 event.

Classification (Amount)	Year
Multi-year (MY) El Niño (10)	1957, 1968, 1976, 1977, 1979, 1986, 1991, 2002, 2014, 2018
Single-year (SY) El Niño (14)	1951, 1963, 1965, 1969, 1972, 1982, 1987, 1994, 1997, 2004, 2006, 2009, 2015, 2019
Multi-year (MY) La Niña (18)	1954, 1955, 1970, 1973, 1974, 1983, 1984, 1988, 1995, 1998, 1999, 2000, 2007, 2010, 2011, 2016, 2020, 2021
Single-year (SY) La Niña (9)	1950, 1956, 1964, 1971, 1975, 2005, 2008, 2017, 2022

48

55 (a)

Classification (Amount)	Year
Multi-year (MY) El Niño (5)	1968, 1976, 1986, 2014, 2018
Single-year (SY) El Niño (19)	1951, 1957, 1963, 1965, 1969, 1972, 1977, 1979, 1982, 1987, 1991, 1994, 1997, 2002, 2004, 2006, 2009, 2015, 2019
Multi-year (MY) La Niña (12)	1955, 1970, 1973, 1974, 1983, 1998, 1999, 2007, 2010, 2016, 2020, 2021
Single-year (SY) La Niña (15)	1954, 1950, 1956, 1964, 1971, 1975, 1984, 1988, 1995, 2000, 2005, 2008, 2011, 2017, 2022

56

57 (b)

58

SPOI	El Niño	La Niña
Multi Year	0.69	−0.63
Single Year	0.10	0.07

Supplementary Table 3. Information about 45 CMIP6 models. Model names, associated institutions, and their corresponding countries/regions are listed.

Model names	Institutes	Countries/regions
ACCESS-CM2	CSIRO-ARCCSS	Australia
ACCESS-ESM1-5	CSIRO	Australia
BCC-CSM2-MR	BCC	China
BCC-ESM1	BCC	China
CAMS-CSM1-0	CAMS	China
CAS-ESM2-0	CAS	China
CESM2-WACCM-FV2	NCAR	United States
CESM2-WACCM	NCAR	United States
CESM2	NCAR	United States
CIESM	THU	China
CMCC-CM2-HR4	CMCC	Italy
CMCC-CM2-SR5	CMCC	Italy
CMCC-ESM2	CMCC	Italy
CanESM5	CCCma	Canada
E3SM-1-0	E3SM-Project, LLNL, UCI, UCSB	United States
E3SM-1-1-ECA	E3SM-Project	United States
E3SM-1-1	E3SM-Project, RUBISCO	United States
EC-Earth3-AerChem	EC-Earth-Consortium	Spain, Italy, Denmark, Finland, Germany, Ireland, Portugal, Netherlands, Sweden, Norway, UK, Belgium
EC-Earth3-CC	EC-Earth-Consortium	
EC-Earth3-Veg-LR	EC-Earth-Consortium	
EC-Earth3-Veg	EC-Earth-Consortium	
EC-Earth3	EC-Earth-Consortium	
FGOALS-f3-L	CAS	China
FGOALS-g3	CAS	China
FIO-ESM-2-0	FIO-QLNM	China
GFDL-ESM4	NOAA-GFDL	United States
GISS-E2-1-G	NASA-GISS	United States
GISS-E2-1-H	NASA-GISS	United States
INM-CM4-8	INM	Russia
INM-CM5-0	INM	Russia
IPSL-CM6A-LR	IPSL	France
KACE-1-0-G	NIMS-KMA	Republic of Korea
KIOST-ESM	KIOST	Republic of Korea
MCM-UA-1-0	UA	United States
MIROC6	MIROC	Japan
MPI-ESM-1-2-HAM	HAMMOZ-Consortium	Switzerland, Germany, UK, Finland
MPI-ESM1-2-HR	HAMMOZ-Consortium	
MPI-ESM1-2-LR	HAMMOZ-Consortium	
MRI-ESM2-0	MRI	Japan
NESM3	NUIST	China
NorCPM1	NCC	Norway
NorESM2-LM	NCC	Norway
NorESM2-MM	NCC	Norway
SAM0-UNICON	SNU	Republic of Korea
TaiESM1	AS-RCEC	Taiwan

62   **Supplementary Table 4. Correlation coefficients between SPOI and various ENSO**

63   **intensity indices.** Correlation coefficients (R) between the SPOI and the Niño3.4,

64   Niño3, and Niño4 indices for El Niño and La Niña events during the period 1950 to

65   2023. Three asterisks denote correlation coefficients that have passed the 99%

66   confidence test.

R (SPOI, Niño)	El Niño	La Niña
Niño3.4	−0.01	0.57[***]
Niño3	−0.08	0.58[***]
Niño4	0.14	0.52[***]

67

68　**Supplementary Table 5. Forecast performance of IRI and SPO for historical**
69　**multi-year El Niño events.** "Year" denotes the decaying year following the first El
70　Niño. IRI provides April-issued probabilities for El Niño in the following NDJ season.
71　An exception is 2002, when forecasts issued in April extended only through JJA and
72　did not cover NDJ. Given the high probability of El Niño in JJA (70%) and the fact that
73　ENSO developed in summer and matured in winter, the event is considered successfully
74　forecasted. SPO-based forecasts depend on the sign of the SPO index value in FMA.
75　IRI data are only available from 2002 onward; earlier years are marked as "N/A",
76　indicating data not available.

| MY El Niño | IRI | | SPOI | |
Year	Probability	Success (>50%)	Value	Success (>0)
1957	N/A	N/A	0.20	Yes
1968	N/A	N/A	−0.48	No
1976	N/A	N/A	1.03	Yes
1977	N/A	N/A	0.25	Yes
1979	N/A	N/A	2.66	Yes
1986	N/A	N/A	2.04	Yes
1991	N/A	N/A	2.24	Yes
2002	70%	Yes	0.12	Yes
2014	66%	Yes	1.15	Yes
2018	48%	No	−0.29	No

77

Supplementary Table 6. Forecast performance of IRI and SPO for historical
multi-year La Niña events. "Year" denotes the decaying year following the first La
Niña. IRI provides April-issued probabilities for La Niña in the following NDJ season.
SPO-based forecasts depend on the sign of the SPO index value in FMA. IRI data are
only available from 2002 onward; earlier years are marked as "N/A", indicating data
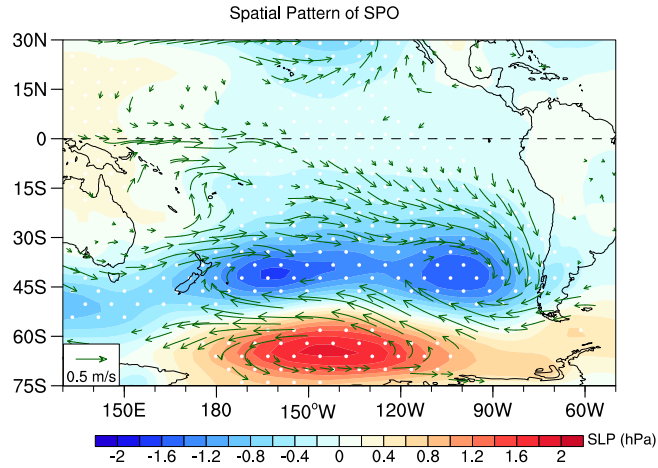not available.

| MY La Niña | IRI | | Year | |
Year	Probability	Success (>50%)	Value	Success (<0)
1954	N/A	N/A	−1.82	Yes
1955	N/A	N/A	−0.62	Yes
1970	N/A	N/A	−1.25	Yes
1973	N/A	N/A	−1.53	Yes
1974	N/A	N/A	0.65	No
1983	N/A	N/A	−0.09	Yes
1984	N/A	N/A	−1.09	Yes
1988	N/A	N/A	−0.04	Yes
1995	N/A	N/A	−0.57	Yes
1998	N/A	N/A	−0.69	Yes
1999	N/A	N/A	−1.27	Yes
2000	N/A	N/A	−1.01	Yes
2007	46%	No	0.02	No
2010	35%	No	−1.42	Yes
2011	23%	No	−0.09	Yes
2016	71%	Yes	0.55	No
2020	37%	No	0.58	No
2021	47%	No	−1.22	Yes

86 **Supplementary Table 7. Forecast performance of IRI and SPO for historical**
87 **single-year El Niño events.** "Year" denotes the decaying year following the first El
88 Niño. IRI provides April-issued probabilities for El Niño in the following NDJ season.
89 SPO-based forecasts depend on the sign of the SPO index value in FMA. IRI data are
90 only available from 2002 onward; earlier years are marked as "N/A", indicating data
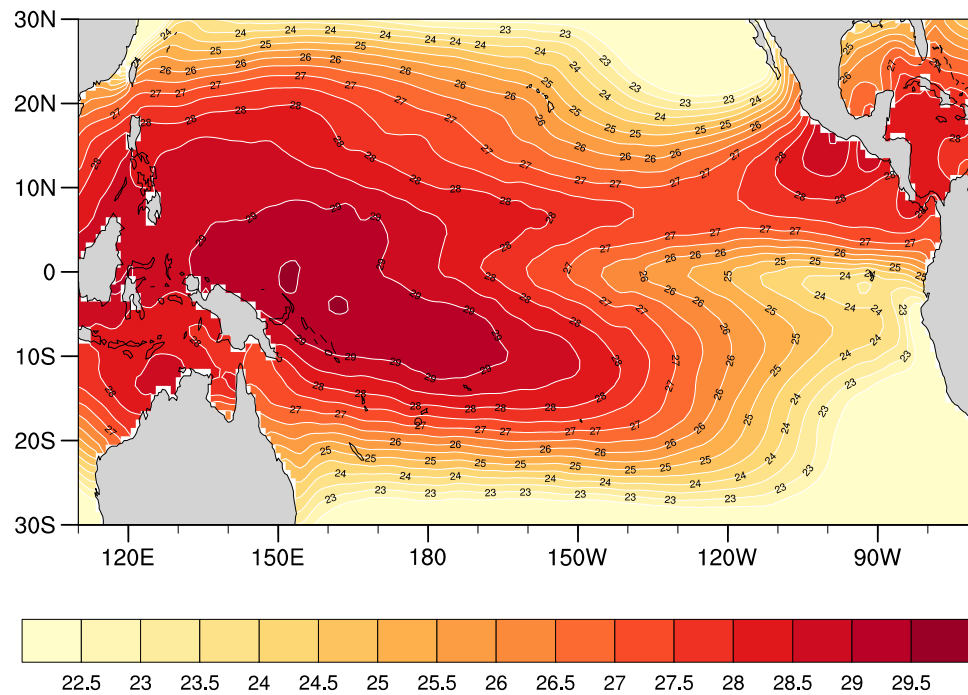91 not available.

| SY El Niño | IRI | | Year | |
Year	Probability	Success (<50%)	Value	Success (<0)
1951	N/A	N/A	−0.53	Yes
1963	N/A	N/A	−1.01	Yes
1965	N/A	N/A	−0.40	Yes
1969	N/A	N/A	0.65	No
1972	N/A	N/A	−0.67	Yes
1982	N/A	N/A	0.07	No
1987	N/A	N/A	−0.02	Yes
1994	N/A	N/A	0.55	No
1997	N/A	N/A	−1.66	Yes
2004	35%	Yes	0.79	No
2006	30%	Yes	−0.48	Yes
2009	30%	Yes	−0.86	Yes
2015	59%	No	−0.40	Yes
2019	51%	No	0.38	No

92

Supplementary Table 8. Forecast performance of IRI and SPO for historical single-year La Niña events. "Year" denotes the decaying year following the first La Niña. IRI provides April-issued probabilities for La Niña in the following NDJ season. SPO-based forecasts depend on the sign of the SPO index value in FMA. IRI data are only available from 2002 onward; earlier years are marked as "N/A", indicating data not available.

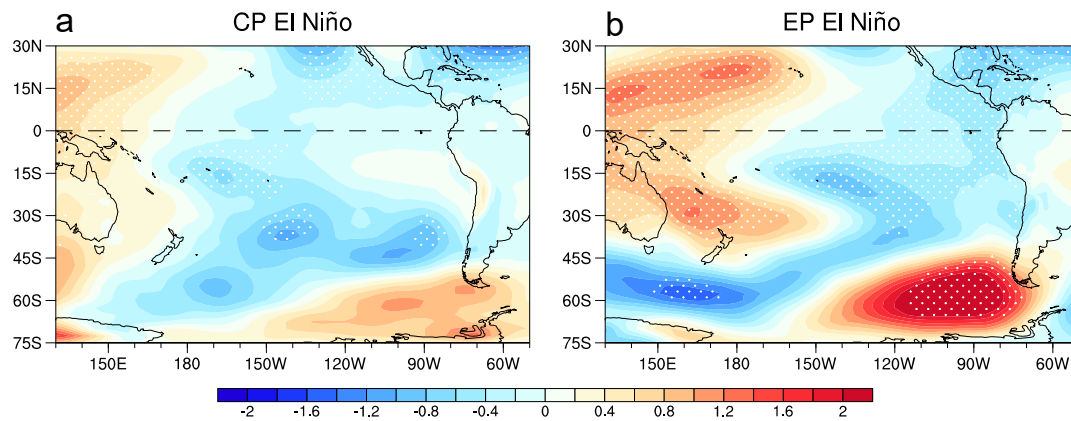| SY La Niña	IRI		Year	
Year	Probability	Success (<50%)	Value	Success (>0)
1950	N/A	N/A	0.77	Yes
1956	N/A	N/A	0.39	Yes
1964	N/A	N/A	0.98	Yes
1971	N/A	N/A	1.03	Yes
1975	N/A	N/A	−0.95	No
2005	5%	Yes	1.09	Yes
2008	20%	Yes	0.69	Yes
2017	12%	Yes	0.57	Yes
2022	52%	No	1.12	Yes

99

Supplementary Figure 1. Spatial pattern of the SPO. SLP (shading; hPa) and 10 m wind (vectors; m/s) anomalies during the boreal spring (FMA) season regressed onto the simultaneous SPO index. Dots indicate regression coefficients that are significant at the 95% confidence level. Only winds significant at the 95% confidence level are shown. Negative SLP anomalies in the northern South Pacific and positive anomalies in the southern South Pacific represent the positive phase of the SPO.
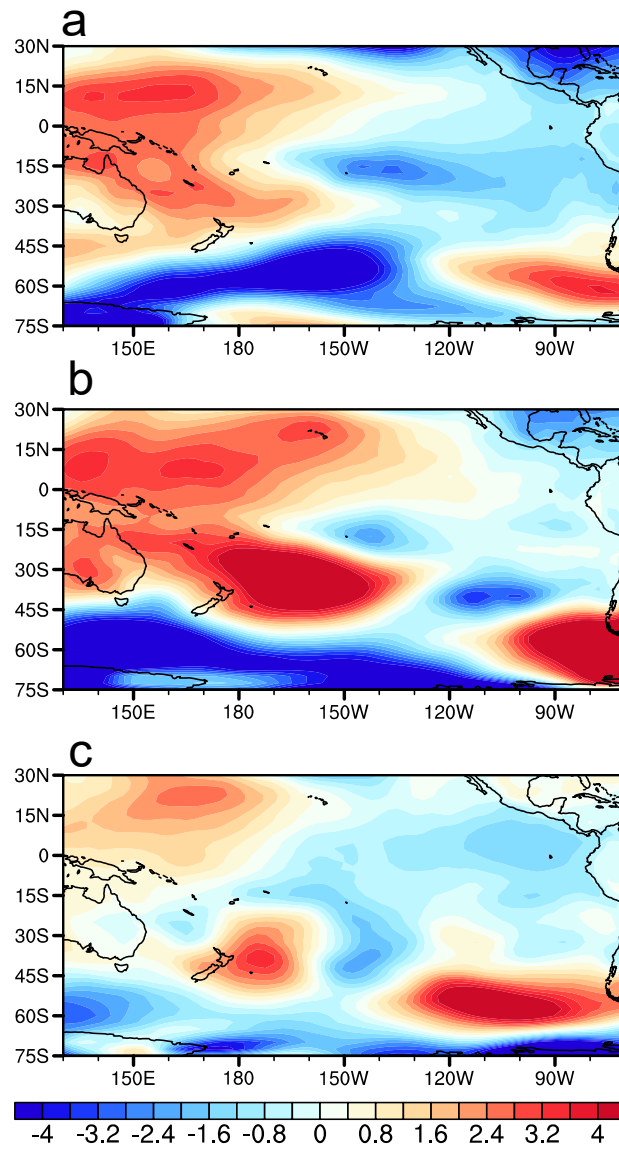
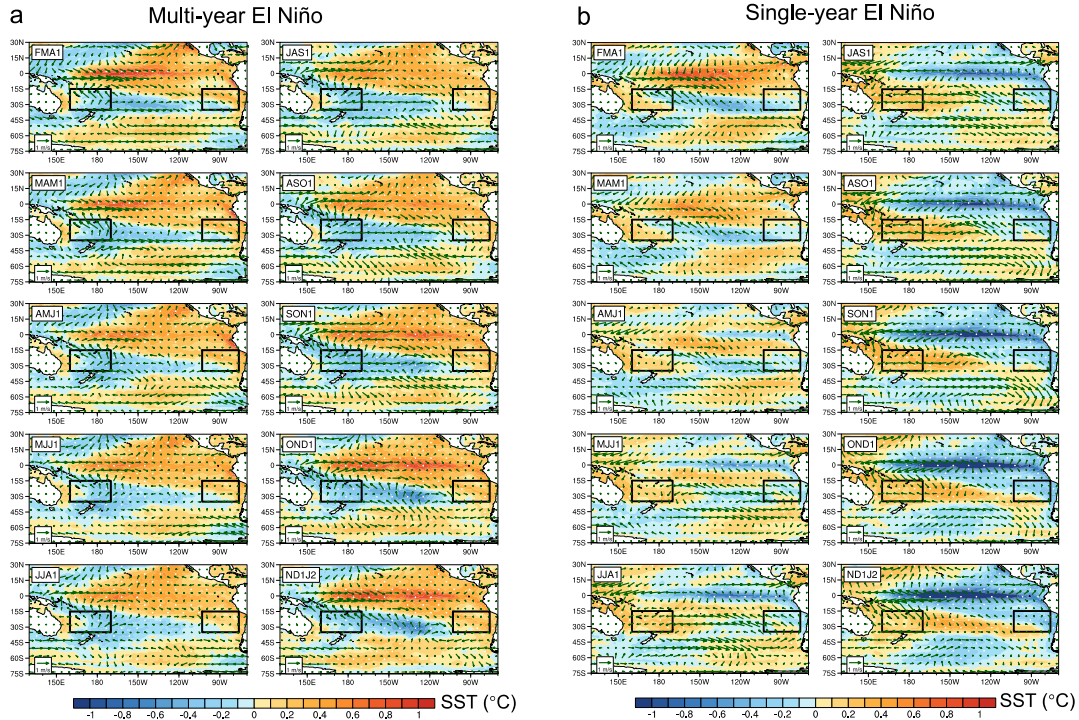**Supplementary Figure 2. Climatological SSTs over the tropical Pacific.**
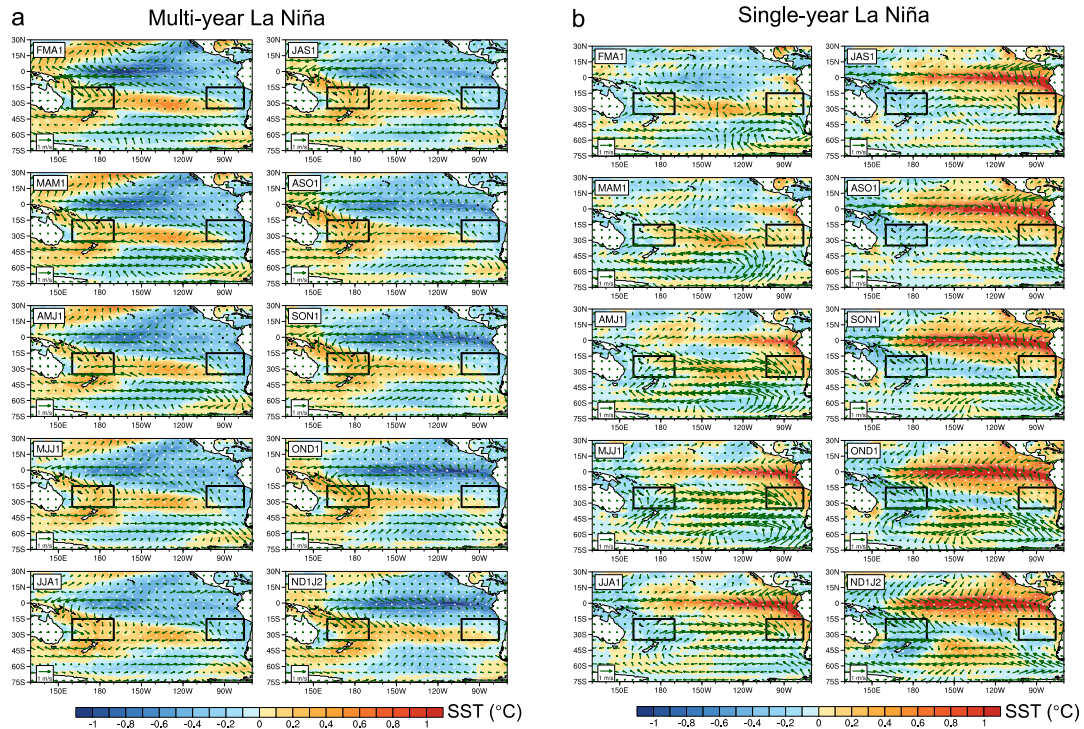Climatological SSTs (shading; °C) during 1950–2023.

Supplementary Figure 3. Contrast in South Pacific SLP patterns between CP and EP El Niño events. Composite SLP anomalies (shading; hPa) in FMA[1] for (a) CP El Niño and (b) EP El Niño. White dots represent the SLP anomalies are significant at the 95% confidence level.
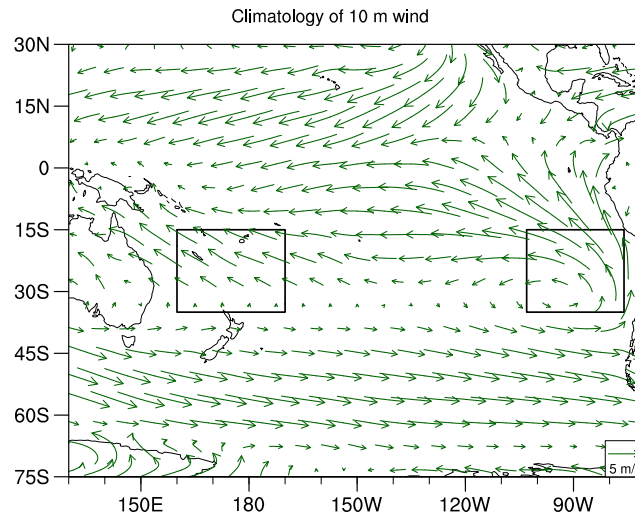
Supplementary Figure 4. SLP anomaly patterns during three major EP El Niño events. SLP anomalies (shading; hPa) for (a) 1982/83, (b) 1997/98, and (c) 2015/16 during the FMA[1] season.

Supplementary Figure 5. Composite seasonal evolutions during the second-year of multi-year and single-year El Niño. Composite monthly SST (shading; °C) and 10 m horizonal wind (vector; m/s) anomalies from the FMA[1] season to the ND[1]J[2] season for (a) MY El Niño and (b) SY El Niño. Black boxes indicate the Southwest and Southeast regions in Fig. 5: 15°S–35°S, 160°E–170°W and 15°S–35°S, 76°W–103°W.

Supplementary Figure 6. Composite seasonal evolutions during the second-year of multi-year and single-year La Niña. Composite monthly SST (shading; °C) and 10 m horizonal wind (vector; m/s) anomalies from FMA^1 season to ND^{1}J^2 season during (a) MY La Niña and (b) SY La Niña. Black boxes are same as that in Supplementary Fig. 5.

Climatology of 10 m wind

131

Supplementary Figure 7. Climatological horizontal wind over the South Pacific.

Climatological 10 m horizonal wind (vector; m/s) during 1950–2023. Black boxes are

same as that in Supplementary Fig. 5.